NIST GCR 07-913

# Determination of Pyrolysis Temperature for Charring Materials

Won Chan Park,
Arvind Atreya
Dept. of Mechanical Engineering
University of Michigan
2202 GGBL
2250 Hayward St.
Ann Arbor, MI 48109
and
Howard R. Baum
U.S. Department of Commerce
Building and Fire Research Laboratory
National Institute of Standards and Technology
Gaithersburg, MD 20899

National Institute of
Standards and Technology
U.S. Department of Commerce

**NIST GCR 07-913**

# Determination of Pyrolysis Temperature for Charring Materials

Prepared for
*U.S. Department of Commerce*
*Building and Fire Research Laboratory*
*National Institute of Standards and Technology*
*Gaithersburg, MD 20899*

By
Won Chan Park
Arvind Atreya
Dept. of Mechanical Engineering
University of Michigan
2202 GGBL
2250 Hayward St.
Ann Arbor, MI 48109
and
Howard R. Baum
U.S. Department of Commerce
Building and Fire Research Laboratory
National Institute of Standards and Technology
Gaithersburg, MD 20899

December 2007

U.S. Department of Commerce
*Carlos M. Gutierrez, Secretary*

National Institute of Standards and Technology
*James M. Turner, Acting Director*

# Notice

**This report was prepared for the Building and Fire Research Laboratory of the National Institute of Standards and Technology under Grant number 60NANB3D1086. The statement and conclusions contained in this report are those of the authors and do not necessarily reflect the views of the National Institute of Standards and Technology or the Building and Fire Research Laboratory.**

**Determination of Pyrolysis Temperature for Charring Materials**

Won Chan Park[1], Arvind Atreya[2] and Howard R. Baum[3]

[1,2]*Department of Mechanical Engineering*
*University of Michigan*
*2202 GGBL 2250 Hayward St. Ann Arbor, MI 48109, USA*

[3]*National Institute of Standards and Technology*
*Building and Fire Research Laboratory*
*Gaithersburg, MD 20899, USA*

*For submission to the 32nd International Symposium on Combustion*

**Colloquium:** *Fire research*

[2] **Corresponding Author**
Tel. : +1-734-647-4790; fax : +1-734- 647-3170
E-mail address : aatreya@umich.edu

**Determination of Pyrolysis Temperature for Charring Materials**


## Abstract

An energy and mass balanced method of determining the pyrolysis temperature is proposed. The concept is to find the pyrolysis temperature that consumes the same amount of energy to produce the same amount of mass when using the pyrolysis front model as when using the finite rate kinetics model for the entire charring process. The resulting pyrolysis temperature has the form of pyrolysis rate weighted average temperature. Comparisons between finite rate kinetics and pyrolysis front models for various boundary conditions, geometries, heats of decomposition, kinetic parameters and assumptions used in the literature were made to assess the proposed method. Models using energy and mass balanced pyrolysis temperature show good agreement with finite rate models and the experiments. Extensive numerical studies on various factors influencing the charring material pyrolysis show that heat flux, sample size, heat of decomposition and kinetic parameters are the most important factors for determining an appropriate pyrolysis temperature. Thermal conductivity, specific heat and density have a lesser effect on the pyrolysis temperature. For practical application, a non-dimensional correlation is developed to determine the appropriate pyrolysis temperature without solving the problem by using the finite rate model. Using this correlation the energy and mass balanced pyrolysis temperature can be determined within 7.6K. These predictions are validated by comparison with measurements of wood cylinder pyrolysis. A good agreement suggests that simpler pyrolysis front models yield practically useful and accurate results given an appropriate pryolysis temperature.



*Keywords: Charring Materials, Pyrolysis, Pyrolysis Temperature, Wood*

**Nomenclature**

| | |
|---|---|
| $A$ | pre-exponential factor $[s^{-1}]$ |
| $C$ | specific heat capacity $[J/kg\,K]$ |
| $E$ | activation energy $[J/mol]$ |
| $k$ | pyrolysis rate $[s^{-1}]$ |
| $m$ | initial mass of charring material $[kg/m^2]$ |
| $n$ | geometric parameter |
| $P$ | pressure $[Pa]$ |
| $Q$ | pyrolysis heat per unit mass of virgin solid $[J/kg]$ |
| $R$ | universal gas constant $[J/molK]$ |
| $T$ | temperature $[K]$ |
| $t$ | time $[s]$ |
| $V$ | pyrolysis front velocity $[m/s]$ |
| $x$ | Cartesian coordinates $[m]$ |
| $Y$ | Solid mass fraction |

$= \frac{1}{\rho_w L}\int_0^L(\rho_a+\rho_c)dx$ for a slab ; $Y = \frac{2}{L^2\rho_w}\int_0^L(\rho_a+\rho_c)x\,dx$ for a cylinder ; & $Y = \frac{3}{L^3\rho_w}\int_0^L(\rho_a+\rho_c)x^2\,dx$ for a sphere.

*Greek Symbols*

| | |
|---|---|
| $\alpha$ | thermal diffusivity $[m^2/s]$ |
| $\gamma$ | char yield fraction |
| $\Delta h$ | pyrolysis heat at reference temperature $T_0$ |
| $\xi$ | integral parameter |
| $\lambda$ | thermal conductivity $[W/m\,K]$ |
| $\rho$ | apparent density $[kg/m^3]$ |
| $L$ | thickness $[m]$ |

*Subscripts*

| | |
|---|---|
| $a$ | virgin solid |
| $c$ | char |
| $f$ | final char |
| $p$ | pyrolysis |
| $s$ | surface |
| $t$ | tar |
| $v$ | volatiles |
| $w$ | initial virgin solid |
| $x, y$ | Cartesian coordinates |
| 0 | reference |

## Introduction

The knowledge of the pyrolysis rate of charring materials like wood is important for the prediction of fire growth because it determines the amount of gaseous fuel generated by the solid for the flames. The process of solid pyrolysis, char formation and growth is quite complex – it involves heat transfer, decomposition reactions, and fuel mass transfer. Numerous models[1-14] have been developed over decades for the analysis and prediction of this charring process. These include models with (i) detailed decomposition kinetics, (ii) one-step kinetics, and (iii) infinite rate kinetics leading to a propagating pyrolysis front that separates char from the virgin material at a specified pyrolysis temperature. While pyrolysis front models circumvent decomposition kinetics, they are attractive because they lead to simpler solutions. This is advantageous because predicting fire growth in multi-story buildings remains a daunting task despite the remarkable growth in computational abilities. Computationally efficient, validated sub-models of component phenomena are sorely needed.

Pyrolysis front models also gain credibility from the facts that: (i) under high temperature environment such as a fire, the kinetics time scale is significantly smaller than the time scale of heat and mass transfer inside the charring solid, and (ii) decomposition kinetics of numerous materials involved in a fire is not well-known. Hence, it is reasonable to model the pyrolysis process by infinite rate kinetics which assumes that the entire chemical reaction occurs abruptly at a constant pyrolysis temperature '$T_p$'. The pyrolysis rate is then controlled by thermal processes and *the choice of the pyrolysis temperature*. The purpose of this paper is to outline a physics-based method of determining an appropriate value of the pyrolysis temperature to improve the accuracy of the pyrolysis front models.

Since the decomposition reaction is characterized by the pyrolysis temperature, the choice of a proper pyrolysis temperature is critical for the accuracy of the infinite rate model. Nevertheless, relatively less attention has been devoted to determining $T_p$ than to developing the model itself. $T_p$ has been either treated as a material property obtainable by some reproducible experiments or a convenient value was assumed from the literature[6,7,9]. Many methods have been used to define the pyrolysis temperature in the

literature. For example, it has been considered as: (i) the temperature at 50% weight loss of a TGA sample[3], (ii) the temperature at the inflection point of a TGA curve[4,5], (iii) the temperature plateau observed during pyrolysis experiments[3], or (iv) estimated from the measured surface temperature and mass loss history[8,10]. Recently, Galgano et al.[11] determined $T_p$ by comparing the pyrolysis front model predictions with the results of the finite rate model. $T_p$ was either taken as the reaction temperature of the finite rate model at the 50% pyrolyzed condition or determined by the condition of equal peak mass loss rate between the finite rate model and the pyrolysis front model. However, the pyrolysis temperature obtained from a constant heating rate TGA curve may not be suitable for a thermally thick charring solid because its heating rate varies with both space and time. Likewise, while $T_p$ as the temperature plateau during the charring process may be considered as a representative value for the overall charring process, such a plateau is not always observed and its value varies with the sample size, shape and boundary conditions. Thus, there is a need for a more general rigorous method of determining the pyrolysis temperature.

In the present study, a physics-based method of finding the pyrolysis temperature is proposed and its performance is evaluated against the finite rate model and experiments for various geometries including 1-D slab, infinitely long cylinder, and sphere. The influence of various factors is also investigated.

**Energy and Mass Balanced Pyrolysis Temperature Concept**

Pyrolysis temperature can be determined by comparing the pyrolysis front model with either the experimental measurements or the finite rate kinetics model. The key question is how to define the matching condition. In this work, $T_p$ is found by ensuring that the same amount of energy is consumed to produce the same amount of mass for the entire charring process of interest by using the pyrolysis front model as when using the finite rate kinetics model.

**Pyrolysis Models**

Consider a "dry" thermally thick charring solid initially at ambient temperature, $T_0$, that is exposed to a constant heat flux on its external surfaces. A schematic of the physical problem is illustrated in Fig.1 for

the 1-D slab geometry. The heat flux is imposed on one side of the slab and the other side is insulated. This renders the half section of twice as thick slab with both sides exposed to the same constant heat flux. When the surface temperature becomes high enough, pyrolysis begins at the surface, and later, the pyrolysis zone advances into the solid leaving behind an insulating char layer. Details of this zone are shown in the inset of Fig.1. Gaseous volatiles generated during pyrolysis are transported to the surface through the porous char matrix. Two types of models are considered: (i) a finite rate decomposition kinetics model that yields a finite thickness of the pyrolysis zone, and (ii) an infinitely fast kinetics model where the pyrolysis zone thickness is zero and a pyrolysis front, associated with a temperature, $T_p$, propagates through the solid. Major assumptions made in the models are: (1) Volatiles and the char matrix are in local thermal equilibrium and the virgin solid is assumed to be impermeable to volatiles flow. (2) Volume of the charring solid remains constant during the charring process, i.e. no char shrinkage. (3) Thermal properties vary with density but are averaged over temperature. Thus, enthalpy is given by: $h(T) = \int_{T_o}^{T} C_p(T)\,dT \approx \bar{C}_p(T - T_o)$.

*Finite Rate Kinetics Model*

During pyrolysis and in finite rate kinetics models, the density of the solid in the pyrolyzing zone changes continuously from the initial density of the virgin solid $'\rho_w'$ to the final density of char $'\rho_f'$. Thus, at any instant, a partially pyrolyzed element may be considered to be a mixture of both char and unpyrolyzed active material. Since zero shrinkage is assumed, all densities are based on the original volume of the solid element yielding the instantaneous solid density as $\rho_s(\vec{x},t) = \rho_a(\vec{x},t) + \rho_c(\vec{x},t)$, where $\rho_a$ and $\rho_c$ are the densities of the active material and char respectively. At $t = 0$, $\rho_s(\vec{x},0) = \rho_a(\vec{x},0) = \rho_w$ and $\rho_c(\vec{x},0) = 0$ and at $t = t_f$, $\rho_s(\vec{x},t_f) = \rho_c(\vec{x},t_f) = \rho_f$ and $\rho_a(\vec{x},t_f) = 0$. In our previous work we have shown that pyrolysis of the virgin solid to char and volatiles may be accurately modeled by a global one step finite rate reaction as long as the correct char yield is used[12]. Char yield, however, can only be determined by a multiple-step parallel reaction model or experiments. Therefore, for the present purpose,

the decomposition rate is described by a 1st order Arrhenius reaction rate with a prescribed char yield $'\gamma' = \rho_f / \rho_w$ as:

$$\partial\rho_a / \partial t = -k\rho_a, \quad \partial\rho_c / \partial t = \gamma k \rho_a \qquad where: \; k = A \cdot \exp(-E/RT) \tag{1}$$

Conservation of mass yields:

$$\frac{\partial \rho_v}{\partial t} + \nabla \cdot \dot{\bar{m}}''_v = -\frac{\partial \rho_s(t)}{\partial t} = (1-\gamma)k\rho_a \;\; ; \;\; where\ \dot{\bar{m}}''_v\ is\ the\ volatile\ mass\ flux\ and\ \partial\rho_v / \partial t \approx 0. \tag{2}$$

Conservation of energy (neglecting the mass of the volatiles in the pores of the charring solid) yields:

$$\left(\rho_a \bar{C}_w + \rho_c \bar{C}_c\right)\frac{\partial T}{\partial t} + \bar{C}_{pv}\,\dot{\bar{m}}''_v \cdot \nabla T = \nabla \cdot \left(\lambda \nabla T\right) + Q(T)k\rho_a \tag{3}$$

Where, $Q(T) = \left(\bar{C}_w - \gamma\bar{C}_c - (1-\gamma)\bar{C}_{pv}\right)(T - T_0) - \Delta h$, is the apparent temperature-dependent heat of pyrolysis and $\Delta h$ is the heat required to generate a unit mass of volatiles at the reference temperature. In Eq.(3), the thermal conductivity 'λ' of the semi-pyrolyzed solid is estimated by a linear combination of virgin solid and char as:

$$\lambda = \left(\frac{\rho_a}{\rho_w}\right)\lambda_w + \left(\frac{\rho_c}{\rho_f}\right)\lambda_c \tag{4}$$

For 1-D slab, cylindrical, and spherical cases, Eq.(3) reduces to:

$$\left(\rho_a \bar{C}_w + \rho_c \bar{C}_c\right)\frac{\partial T}{\partial t} + \bar{C}_{pv}\,\dot{\bar{m}}''_v \frac{\partial T}{\partial x} = \frac{1}{x^n}\frac{\partial}{\partial x}\left(x^n \lambda \frac{\partial T}{\partial x}\right) + Q(T)k\rho_a \tag{5}$$

Where, $n = 0$ represents a slab, $n = 1$ a cylinder, and $n = 2$ a sphere. Also, $\dot{\bar{m}}''_v(\bar{x}, t) = \int_0^x (1-\gamma)k\rho_a \cdot \left(\frac{\xi}{x}\right)^n \cdot d\xi$ .

*Infinite Rate Kinetics* (*Pyrolysis Front*) *Model*

For the pyrolysis front model, the solid is divided into two zones, virgin solid and char, by an isothermal pyrolysis front. For simplicity, virgin solid is assumed to be impermeable to volatiles flow. Therefore, the volatiles convection term is ignored in the following energy equation:

$$\frac{\partial T}{\partial t} = \frac{\alpha_w}{x^n}\frac{\partial}{\partial x}\left(x^n \frac{\partial T}{\partial x}\right) \qquad ; \qquad 0 < x < x_p(t) \tag{6}$$

Where, $\alpha_w = \frac{\lambda_w}{\rho_w \bar{C}_w}$ is the virgin solid thermal diffusivity and $x_p(t)$ is the location of the pyrolysis front.

The energy equation for the char, however, includes the thermal effect of volatiles convection.

$$\frac{\partial T}{\partial t}+\frac{\bar{C}_{pv}}{\bar{C}_c}\frac{\dot{m}_v''}{\rho_c}\frac{\partial T}{\partial x}=\frac{\alpha_c}{x^n}\frac{\partial}{\partial x}\left(x^n\frac{\partial T}{\partial x}\right) \qquad ; \qquad x_p(t)<x<L \tag{7}$$

Where, $\alpha_c=\dfrac{\lambda_c}{\rho_f\cdot\bar{C}_c}$ is the char thermal diffusivity, $\dot{m}_v''(\vec{x},t)=\rho_w\cdot(1-\gamma)\cdot\left(\dfrac{x_p(t)}{x}\right)^n\dfrac{dx_p}{dt}$ is the volatiles mass flux. The location of the pyrolysis front is determined by the conditions:

$$\lambda_c\left.\frac{dT}{dx}\right|_c-\lambda_w\left.\frac{dT}{dx}\right|_w=\left(Q(T_p)\cdot\rho_w\right)\cdot\frac{dx_p(t)}{dt} \qquad and \qquad T=T_p \tag{8}$$

*Determination of the Pyrolysis Temperature*

Consider an instantaneous snapshot of the pyrolysis process. The inset in Fig.1 shows the variation in various quantities during pyrolysis and the pyrolysis front approximation. The location of the pyrolysis front is determined by the value of the pyrolysis temperature $'T_p'$ and it may not lie in the middle of the pyrolysis zone, as shown. Presumably, the pyrolysis front is somewhere within this reaction zone, but we do not know this to be true *a priori*. The control volume $'\Delta x'$ is chosen to be thick enough to include both the entire finite rate pyrolysis zone and the pyrolysis front. As the pyrolysis front passes through $'\Delta x'$ initially consisting of the virgin material at time '$t$', it is converted to char at '$t+\Delta t$' (assuming no shrinkage). To determine the energy and mass balanced $T_p$, we first note that mass is automatically balanced as the sample goes from $\rho_w$ to $\rho_f$ for constant $\gamma$. To equalize the energy consumed by the finite-rate kinetics and the pyrolysis front models, we note that there is no difference in the energy content of the remaining char as long as the energy imparted to the volatiles is the same for the two models.

The rate at which energy is acquired by the pyrolysis gases according to the finite rate kinetics model is:

$$\dot{H}(t) = (1-\gamma)\int_x^{x+\Delta x} k\rho_a(\xi,t)\,\bar{C}_{pv}\left(T(\xi,t)-T_o\right)d\xi = (1-\gamma)\int_0^L k\rho_a(\xi,t)\,\bar{C}_{pv}\left(T(\xi,t)-T_o\right)d\xi. \tag{9}$$

The second equality is true because there is no more *creation* of volatiles outside $\Delta x$. The corresponding expression for the pyrolysis front model is:

$$\dot{H}(t) = \rho_w(1-\gamma)\int_x^{x+\delta x} \delta\left(\xi-\xi_p(t)\right)\frac{d\xi_p}{dt}\,\bar{C}_{pv}\left(T(\xi,t)-T_o\right)d\xi = \rho_w L(1-\gamma)\bar{C}_{pv}\left(\tilde{T}_p(t)-T_o\right)\frac{dx_p(t)}{dt}. \qquad (10)$$

For the second equality, the integration is again extended over the entire spatial domain and properties of the Dirac delta function are used. Equating equations (9) and (10) will give us the time-dependent pyrolysis temperature $'\tilde{T}_P(t)'$ which is practically not very useful. Thus, integrating over the entire time that the charring process occurs yields a physically and computationally useful 'mass and energy balanced' pyrolysis temperature $T_p$ as:

$$T_p = \frac{1}{\rho_w L}\int_0^{t_f}\int_0^L T(x,t)\,k\,\rho_a\,dx\,dt\,. \qquad (11)$$

Thus, $'T_p'$ is the decomposition rate weighted average temperature for the entire charring process.

**Results and Discussion**

The models presented above were numerically solved and compared to determine the energy and mass balanced pyrolysis temperature for various sample thicknesses, shapes and boundary conditions. Material properties used are listed in Table 1.

*Effect of boundary conditions:*

The finite rate model (model-A) and two pyrolysis front models one using the energy and mass balanced pyrolysis temperature (model-B1) and the other using a constant pyrolysis temperature (model-B2) are compared for four different boundary conditions in Fig.2. For model-B1, $T_p$ was obtained by energy and mass balance from model-A for each boundary condition (see figure caption). For model-B2, same $T_p\,(=678K)$ is used for all boundary conditions, which is the $T_p$ for model-B1 found for the no heat loss condition. As the surface heat loss increases, $T_p$ for model-B1 decreases and the difference between the models B1 and B2 increases.

Model-A predicts earlier surface pyrolysis and a gradual increase in the pyrolysis rate, whereas, models B1 and B2 show a sudden increase in the pyrolysis rate when the surface temperature reaches the pyrolysis temperature. This implies that pyrolysis temperature models are inadequate for predicting the

ignition temperature. They predict that pyrolysis temperature is, in fact, the ignition temperature. In the final pyrolysis stage, models B1 and B2 show a sudden decrease in the mass loss rate when the pyrolysis front reaches the insulated boundary. Models B1 and B2 agree better with model-A for the no heat loss boundary condition than for the radiation and convection boundary condition because the faster heating rate and higher material temperature results in a thinner pyrolysis zone. Model-B1 shows good agreement for the overall mass loss rate with model-A for all boundary conditions and the pyrolysis is completed in the same amount of time. Whereas, model B2 predicts 14% longer pyrolysis time for radiation and convection heat loss boundary condition [Fig.2a]. As the difference between $T_p$ for models B1 and B2 becomes smaller, the mass loss rate difference between the two pyrolysis front models reduces. Therefore, it is important to use a proper $T_p$ for the pyrolysis front model for different boundary conditions. These results show that enforcing energy and mass balance is an effective method of finding the proper pyrolysis temperature.

*Effect of geometry*

The pyrolysis of 1-D cylinder and sphere was analyzed using the pyrolysis front model (B1) and finite rate model (A). Radiation and convection surface boundary condition was used to represent realistic situations. As shown in Fig. 3, the pyrolysis front model (B1) generated a smaller peak mass loss rate than the finite rate model (A). The pyrolysis front model (B1) predicted a slightly longer pyrolysis time than the finite rate model (A). Unlike the slab cases, a sudden decrease of mass loss rate for the pyrolysis front model (B1) does not occur because for curved geometries pyrolysis front area which is proportional to the radius or the square of the radius, decreases as pyrolysis zone approaches the center, while it remains constant for the slab geometry. The mass loss rate is the product of the pyrolysis front area and the speed of the front advance. In addition, since curved geometries have larger surface to volume ratio than the slab, total pyrolysis time is much shorter than the slab case [Fig.2a].

*Effects of Various Parameters on the Pyrolysis Temperature*

The effect of various parameters was studied to determine their influence on the energy and mass balanced pyrolysis temperature. These parameters were individually varied around their base values to cover the variation in the literature and energy and mass balanced pyrolysis temperature was determined by comparing the pyrolysis front model with the finite rate model. For this investigation, 1-D slab geometry illustrated in Fig. 1 was used with one side insulated and the other exposed to a constant heat flux with radiation and convection heat loss. The sample thickness was $1cm$. Material properties, reaction heat and kinetic parameters for the base condition are listed in Table1.

*Physical parameters*

Heat Flux: Figure 4 shows that for fire-level heat fluxes of 2 to $10\ W/cm^2$, $T_p$ increases with the heat flux from 617.9 K to 667.8 K. At higher heat fluxes, the solid is heated faster and pyrolysis occurs at higher temperatures resulting in a higher $T_p$. The influence of the heat flux on $T_p$ is significant and the curve seems to suggest that as the heat flux is increased even further some asymptotic value of the pyrolysis temperature may be reached.

Sample Size: Figure 4 also shows the effect of sample thickness. A range from $0.1\ to\ 2cm$ was used. In this range, $T_p$ changed from 607.0K to 697.8K. Thinner materials lead to higher pyrolysis temperatures due to higher heating rates – a condition similar to higher heat fluxes.

Thermal Properties: The effect of various thermal properties on energy and mass balanced pyrolysis temperature is shown in Fig. 5. $T_p$ varies from 626.8K to 654.6K with char thermal conductivity ranging from $0.08\ W/mK\ to\ 0.7\ W/mK$. Char conductivity affects the pyrolysis temperature because the heat transfer from the surface to the pyrolysis zone is proportional to it. Higher char conductivity increases the heating rate in the pyrolysis zone and hence the pyrolysis temperature. In contrast, the effect of virgin solid conductivity is negligible.

The effect of specific heat is interesting. A large specific heat of either the char or the virgin solid is expected to decrease the heating rate and hence the pyrolysis temperature. This happens for char but the virgin solid shows an opposite trend. Looking further, we find that the apparent temperature-dependent

heat of pyrolysis $Q(T)$ in Equ.(3) becomes less endothermic with large $\bar{C}_w$ ,whereas, $\bar{C}_C$ has an opposite sign. The combined effect for $\bar{C}_w$ is that $T_p$ is weakly proportional to $\bar{C}_w$ as shown in Fig. 5(b). The effect of density is similar. Larger density will increase the thermal load and reduce the heating rate resulting in slower pyrolysis and lower pyrolysis temperatures. As shown in Fig. 5(c), $T_p$ drops from 646.8 K to 628.8 K over a $\rho_w$ range of $400\ kg/m^3$ to $800 kg/m^3$. Also note that larger $\rho_w$ leads to a smaller char yield $\gamma$ for constant $\rho_f$ which will make *Q(T)* less endothermic unless $\bar{C}_{pv} > \bar{C}_c$, which is the case. Likewise, larger char density will reduce the heating rate and result in larger $\gamma$. For $\bar{C}_{pv} > \bar{C}_c$, larger $\gamma$ makes the reaction less endothermic increasing the pyrolysis temperature. These conflicting effects render a weak dependence of $T_p$ on char density. From Figs. 5(a,b,c) it is clear that $T_p$ is nearly independent of $\alpha_w = \lambda_w/\rho_w\bar{C}_w$ and the primary dependence on $\alpha_c$ is through $\lambda_c$.

The effect of pyrolysis heat is shown in Fig. 5(d). Pyrolysis temperature is found to be inversely proportional to the endothermic reaction heat ($\Delta h$). Here ($\Delta h$) is the reaction heat at reference temperature, not at reaction temperature. The actual reaction becomes exothermic ($Q(T) > 0$) for small $\Delta h$ because the specific heat of reactant is larger than the products. For these exothermic cases ($\Delta h < 100\frac{kJ}{kg}$), $T_p$ increases sharply.

*Kinetic parameters*

Compared to the physical parameters, kinetic parameters, i.e. activation energy ($E$) and pre-exponential constant ($A$), directly influence the pyrolysis rate. Hence, strong relations exist between $T_p$ and the kinetic parameters, as shown in Fig. 6. $T_p$ varies by more than 100K for published ranges of $E$ and $A$. $T_p$ increases linearly with the activation energy and decreases exponentially with increase in the pre-exponential constant.

*Estimation of the Energy and Mass Balanced Pyrolysis Temperature*

In the above parametric study, the energy and mass balanced pyrolysis temperature was obtained by comparing the pyrolysis front model with the finite rate model. Clearly, a more convenient method of estimating $T_p$ must be found. Thus, the understanding gained above is summarized into a non-dimensional correlation. We start by normalizing Equ. (11) which, if solved, will yield the desired $T_p$. We choose a reference temperature $T_R$ close to the expected $T_p$ such that $\delta T \equiv (T - T_R) \ll T_R$ and define a characteristic thickness $L = \frac{volume}{surface\ area}$. Thus, $L = thickness$ for a slab; $L = \frac{radius}{2}$ for a cylinder and $L = \frac{radius}{3}$ for a sphere. An excellent approximation for the reaction rate is: $k \approx A^*\left(1 + E\,\delta T / R T_R^2\right)$ where, $A^* = A e^{-E/RT_R}$. Thus, Equ. (11) is rewritten as:

$$\frac{T_p}{T_R} = e^{-\phi} \int_0^1 \int_0^{t_f/t'_f} \left(1 + \frac{E\,\delta T}{R T_R^2}\right)\left(\frac{\rho_a}{\rho_w}\right)\left(\frac{T(\xi,\tau)}{T_R}\right) d\tau\, d\xi\,;\ where\ \tau = \frac{t}{t'_f}\ \&\ \xi = \frac{x}{L} \tag{12}$$

Here $t'_f$ is not *a priory* known. It is chosen from the physical parameters such that $t'_f \sim t_f$ to make the integral of order unity. The above parametric study shows that $t'_f \propto \Delta h\, L\, \rho_w / \dot{q}''$, which leads to the non-dimensional parameter $\phi = \frac{E}{RT_R} - \ln\left(\frac{A \Delta h L \rho_w}{\dot{q}''}\right)$ in Equ.(12). It is important to note that $\phi$ includes the effect of all the major variables that influence the pyrolysis temperature and has the correct dependences. The integral in Equ.(12) is not solved but it is used to motivate the choice of the non-dimensional parameters $T_p/T_R$ *and* $\phi$ shown in Fig.7. Interestingly, a linear relationship is observed which is not obvious from Equ. (12). The symbols in Fig. 7 represent the energy and mass balanced $T_p$ determined in the above parametric study by individually varying each parameter for a slab, cylinder and sphere, as well as, nine mixed cases listed in Table 2. Thus given the basic variables and the material properties, an appropriate energy and mass balanced pyrolysis temperature can be determined from Fig. 7 within 7.6 K and used in the pyrolysis front model without sacrificing accuracy of the model prediction.

*Comparison with Experiments on Wood*

As application of the models, beech wood cylinder pyrolysis was numerically solved and compared with experimental measurements of Di Blasi et al. [15]. In the experiments, beech wood cylinders of 2 cm radius and 4 cm length were exposed to thermal radiation of $40\ to\ 80\ kW/m^2$. Details of the experimental and numerical simulation conditions are described in Ref. [11, 15]. Fig.8 shows the experimental data and calculations using the finite rate model (A) and the pyrolysis front model (B1). The mass and energy balanced pyrolysis temperatures obtained from the correlation are listed in the figure caption. They vary from 642K to 667K. Comparison with both the change in the solid mass fraction (Y) and its rate of change (dY/dt) are shown. It is seen that the pyrolysis front model agrees well with the finite rate model. Further, both models agree equally well with the measurements. The discrepancy in the final stages of pyrolysis is believed to be caused by the volatiles convection term because its effect becomes more significant in the final stage due to thicker char layer and larger temperature difference between the pyrolysis zone and the surface. Thus, the value of the volatiles specific heat used in the models may be too large. Another possibility is cracking of the char matrix that may allow the volatiles to leave without complete heat transfer with the char, as assumed in the models. Char cracking may also change the radiation boundary condition. Given these complications, the overall prediction of the models is equally acceptable for both the pyrolysis front and the finite rate model. The mass loss rate (dY/dt) predictions also show good agreement with the measurements for high heat flux boundary conditions $(69,\ 80kW/m^2)$ and poor agreement for low heat flux boundary conditions $(49,\ 40kW/m^2)$ for both models.

**Conclusions**

A method of determining the pyrolysis temperature by enforcing energy and mass balance is proposed and validated by comparison with the decomposition kinetics model and the experiments. This pyrolysis temperature has the form of pyrolysis rate weighted average temperature for the entire charring process. The pyrolysis front model using the energy and mass balanced pyrolysis temperature shows good agreement with the finite rate model for various geometries, boundary conditions and properties. A comparison between the energy and mass balanced pyrolysis temperature and a constant pyrolysis

temperature indicates the importance of choosing the proper pyrolysis temperature to improve the accuracy of the pyrolysis front models. Extensive numerical studies on various factors influencing pyrolysis showed that heat flux, sample size, heat of pyrolysis and kinetic parameters are the most important for determining an appropriate pyrolysis temperature. Further, this parametric study is used to derive a non-dimensional parameter to determine the appropriate pyrolysis temperature without solving the charring problem by using the finite rate model. An appropriate pyrolysis temperature, for a given problem, can now be determined within 7.6 K by the proposed correlation. Use of this method to predict the results of wood cylinder pyrolysis experiments validate its applicability and the proposed energy and mass balanced pyrolysis temperature concept.

**Acknowledgments**

The research at the University of Michigan was supported by NIST grant # 3D1086.

**References**

1. A. Atreya, *Pyrolysis, Ignition and Flame Spread on Horizontal Surfaces of Wood*, Ph.D. thesis, Harvard University, Cambridge, MA, 1983.
2. C. Di Blasi, C. Branca, *Industrial & Engineering Chemistry Research* 40 (2001) 5547–5556.
3. Desrosiers, R. J. Lin, *Solar Energy* 33, No. 2. (1984) 187–196.
4. J.E.J. Staggs, *Fire and Materials* 24 (2000) 305–308.
5. J.E.J. Staggs, *Polymer Degradation and Stability* 82 (2003) 297–397.
6. A. Atreya, H.R. Baum, *Proceedings of the Combustion Institute* 29 (2002) 227–236.
7. H.R. Baum, A. Atreya, *Proceedings of the Combustion Institute* 31 (2007) 2633–2641.
8. F. Jia, E. R. Galea, and M. K. Patel, *Fire and Materials* 23 (1999) 71–78.
9. Y. Chen, M.A. Delichatsios, V. Motevalli, *Combustion Science and Technology* 88 (1993) 309–328
10. B. Moghtaderi, V. Novozhilov, D. Fletcher, J. H. Kent, *Fire and Materials* 21 (1997) 7–16.
11. A. Galgano, C. Di Blasi, *Combustion Science and Technology* 177 (2005) 279-303.

12. Won Chan Park, A. Atreya, and H.R. Baum, *Proceedings of the Combustion Institute* 31 (2007) 2643–2652.

13. I. S. Wichman, A. Atreya, *Combustion and Flame* 68 (1987) 231–247.

14. C. K. Lee, R. F. Chaiken, J. M. Singer, *Proceedings of the Combustion Institute* 16 (1974) 1459–1470.

15. C. Di Blasi, C. Branca, A. Santoro, E. G. Hernandez, *Combustion and Flame* 124 (2001) 165-177.

Table 1: Material properties and kinetic constants

| Property | Value | Source | Property | Value | Source |
|---|---|---|---|---|---|
| $\rho_w$ | 676 kg/m$^3$ | [3] | $A$ | $2.5\times10^8$ s$^{-1}$ | [3] |
| $\rho_c$ | 162.24 kg/m$^3$ | [3] | $\Delta h$ | 248.3 kJ/kg | [1] |
| $C_w$ | 1.492 kJ/kg K | [14] | $\lambda_w$ | 0.189 W/m K | [3] |
| $C_c$ | 0.787 kJ/kg K | [3] | $\lambda_c$ | 0.117 W/m K | [14] |
| $C_v$ | 1.114 kJ/kg K | [3] | $R$ | $8.314\ J/mol\ K$ | |
| $E$ | 125.58 kJ/mol | [3] | $T_0$ | 298.15 K | |

Table 2: Description of mixed cases; Values different from the base case are printed in bold fonts.

| | heat flux $(W/cm^2)$ | $L$ $(m)$ | $\Delta h$ $(kJ/kg)$ | $E$ $(kJ/mol)$ | $A$ $(1/s)$ |
|---|---|---|---|---|---|
| case 0 (base) | 3 | 0.01 | 248.3 | 125.58 | 2.50E+08 |
| case 1 | **5** | **0.005** | 248.3 | 125.58 | 2.50E+08 |
| case 2 | **2** | **0.005** | 248.3 | 125.58 | 2.50E+08 |
| case 3 | **5** | **0.02** | 248.3 | 125.58 | 2.50E+08 |
| case 4 | **8** | **0.02** | 248.3 | 125.58 | 2.50E+08 |
| case 5 | 3 | 0.01 | 248.3 | **115** | **1.50E+09** |
| case 6 | 3 | 0.01 | 248.3 | **115** | **3.00E+07** |
| case 7 | 3 | 0.01 | 248.3 | **135** | **3.00E+07** |
| case 8 | 3 | 0.01 | 248.3 | **135** | **2.00E+09** |
| case 9 | 3 | 0.01 | **500** | **125** | **1.50E+09** |

**List of figures**

**Figure 1:** Schematic illustration of a pyrolyizing charring solid for 1-D slab geometry.

**Figure 2:** Solid mass loss rate [$dY/dt$, where: $Y = \frac{1}{\rho_w L}\int_0^L(\rho_a + \rho_c)dx$] for $1cm$ thick slab exposed to 3 $W/cm^2$ external radiation. Comparison of finite rate model with the pyrolysis front model for various boundary conditions: model A – finite rate model; model B1 – pyrolysis front model using mass and energy balanced $T_p$; model B2 – constant pyrolysis temperature ($T_p = 678\ K$). Cases: (a) radiation and convection heat loss ($T_p for\ B1 = 632.9K$); (b) radiation heat loss ($T_p for\ B1 = 638.7K$); (c) convection heat loss ($T_p for\ B1 = 667K$); (d) no heat loss ($T_p for\ B1 = 678K$)

**Figure 3:** Solid mass loss rate [$\boldsymbol{dY/dt}$, **where**: $\boldsymbol{Y = \frac{2}{L^2\rho_w}\int_0^L(\rho_a + \rho_c)x\,dx}$. **for a cylinder** & $\boldsymbol{Y = \frac{3}{L^3\rho_w}\int_0^L(\rho_a + \rho_c)x^2\,dx}$. **for a sphere**] for $\boldsymbol{1cm}$ radius samples exposed to $\boldsymbol{3W/cm^2}$ external radiation, Comparison of finite rate model (A) with mass & energy balanced $\boldsymbol{T_p}$ model (B1) for (a) cylinder $(\boldsymbol{T_p = 655.9K})$(b) sphere($\boldsymbol{T_p = 669.9K}$).

**Figure 4:** Effect of heat flux and sample thickness on energy and mass balanced pyrolysis temperature.

**Figure 5:** Effect of thermal properties of virgin material & char on mass & energy balanced pyrolysis temperature.

**Figure 6:** Effect of the activation energy & pre-exponential constant on energy and mass balanced $T_p$.

**Figure 7:** Non-dimensional correlation of finite rate and pyrolysis front calculations for a wood slab, cylinder & sphere for estimating the pyrolysis temperature from primary variables namely: Activation energy ($E$); pre-exponential factor ($A$); heat of pyrolysis ($\Delta h$); characteristic thickness ($L$); virgin solid density ($\rho_w$); external heat flux ($\dot{q}''$); and a random mix of these variables. Symbols represent these variables. They were systematically varied over the range available in the literature for wood. The dotted line is the best fit correlation. The correlation is insensitive to the value of the reference temperature ($T_R$) chosen. In the above plot, $T_R$ was varied between 600K and 700K. The standard deviation of the correlation is 7.6K.

**Figure 8:** Comparison of models with the experimental measurements of [15]. Symbols – experiments; Red line – finite rate model A; Green line – pyrolysis front model B1. Y → solid mass fraction, dY/dt → solid mass loss rate. Mass & energy balanced $T_p$ for B1: $\boldsymbol{642K \leftrightarrow 40\frac{kW}{m^2}; 650K \leftrightarrow 49\frac{kW}{m^2}; 662K \leftrightarrow 69\frac{kW}{m^2}; 667K \leftrightarrow 80\frac{kW}{m^2}}$.

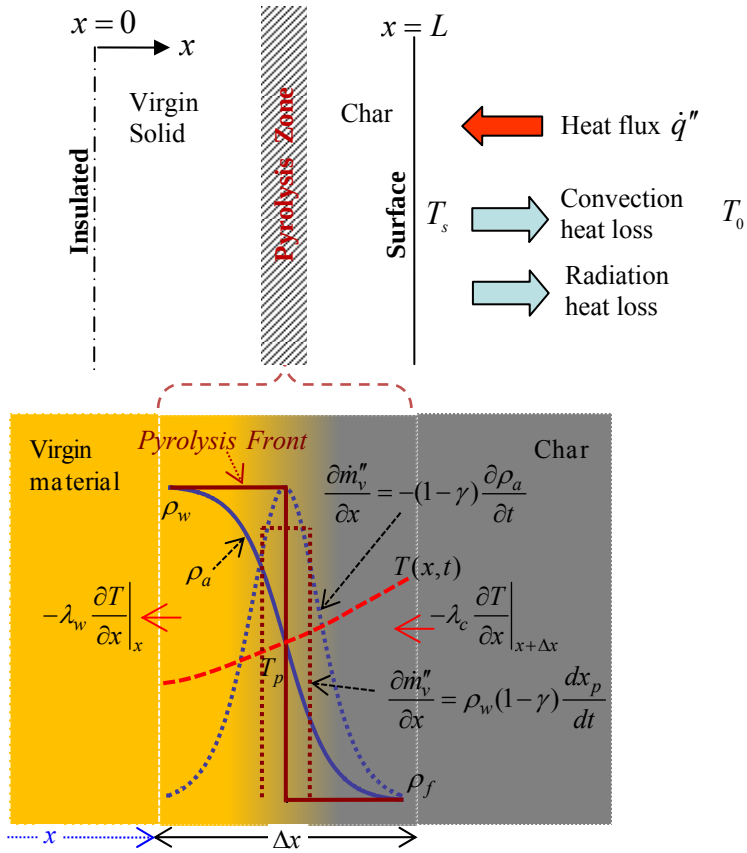


**Figure 1:** Schematic illustration of a pyrolyizing charring solid for 1-D slab geometry.

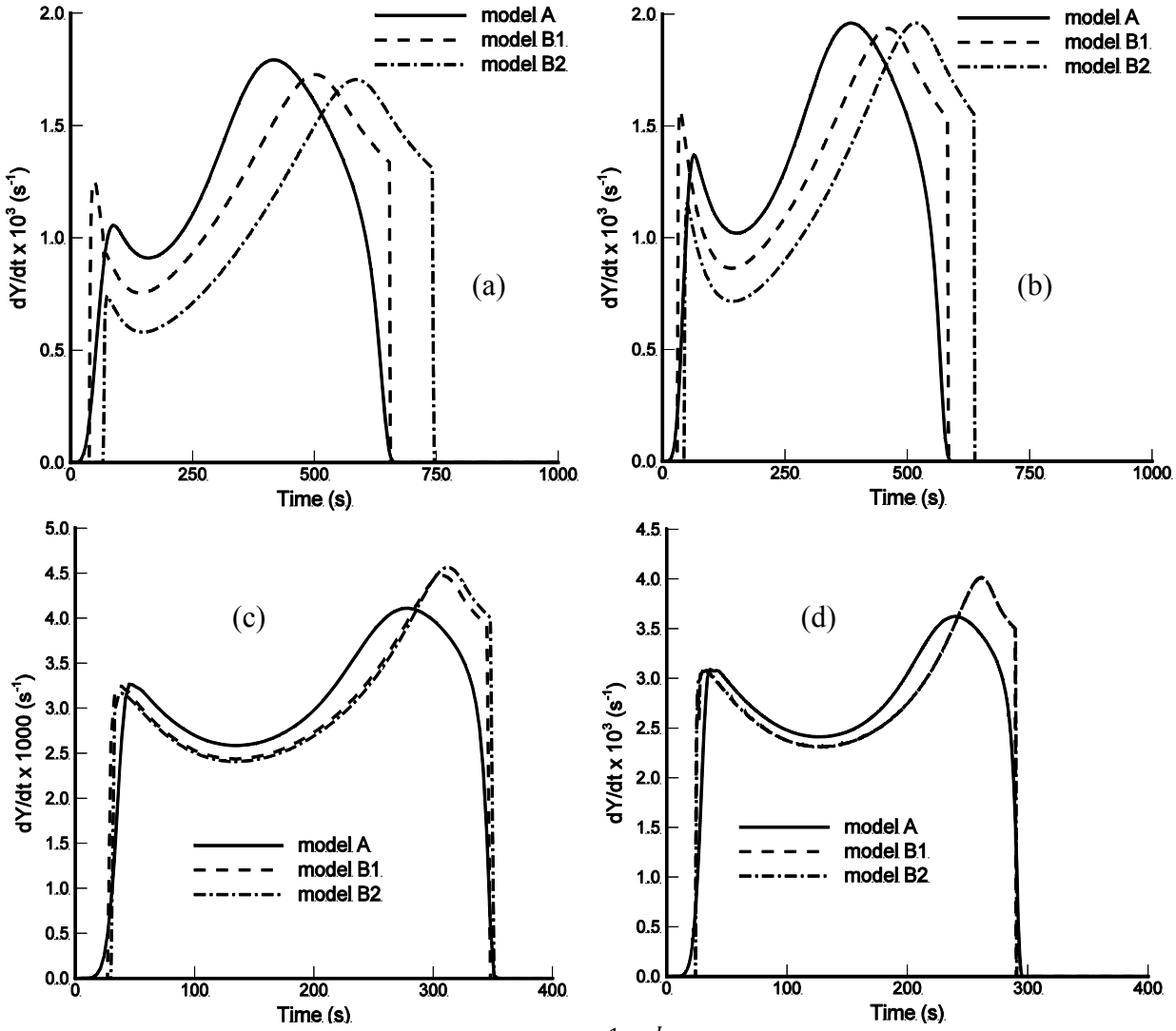


**Figure 2:** Solid mass loss rate $[dY/dt, \text{where: } Y = \frac{1}{\rho_w L}\int_0^L(\rho_a + \rho_c)dx]$ for a $1cm$ thick slab exposed to $3\ W/cm^2$ external radiation. Comparison of finite rate model with pyrolysis front model for various boundary conditions: model A – finite rate model; model B1 – pyrolysis front model using mass and energy balanced $T_p$; model B2 – constant pyrolysis temperature ($T_p = 678\ K$). Cases: (a) radiation and convection heat loss ($T_p for\ B1 = 632.9K$) ; (b) radiation heat loss ($T_p for\ B1 = 638.7K$) ; (c) convection heat loss ($T_p for\ B1 = 667K$); (d) no heat loss ($T_p for\ B1 = 678K$)

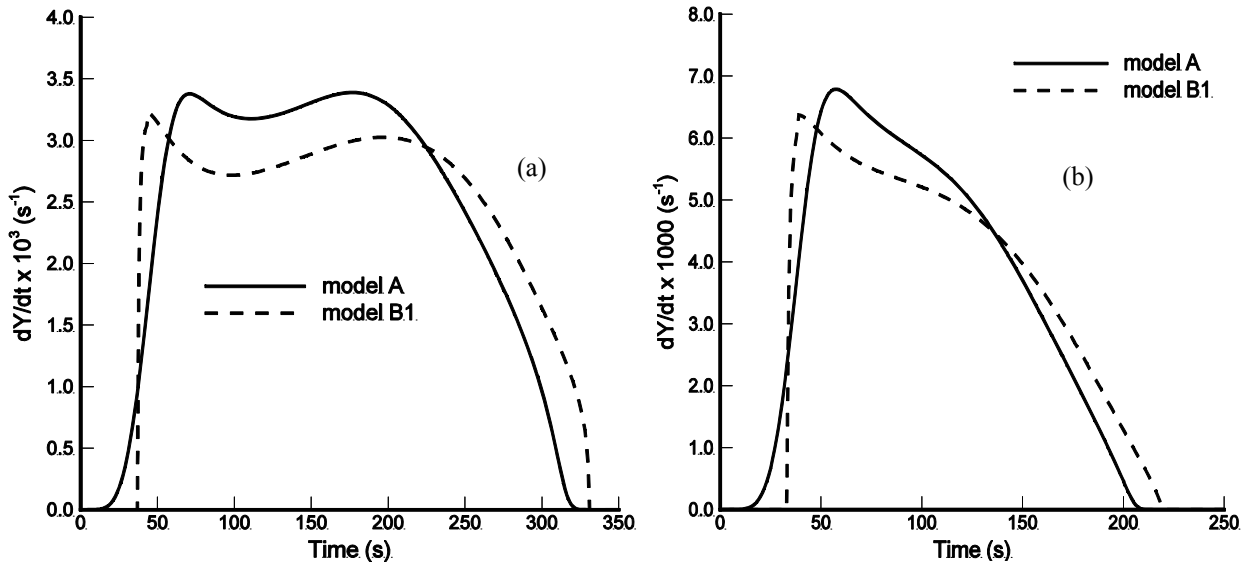


**Figure 3:** Solid mass loss rate $[dY/dt$, where: $Y = \frac{2}{L^2\rho_w}\int_0^L(\rho_a + \rho_c)x\,dx.$ for a cylinder & $Y = \frac{3}{L^3\rho_w}\int_0^L(\rho_a + \rho_c)x^2\,dx.$ for a sphere] for $1cm$ radius samples exposed to $3W/cm^2$ external radiation, Comparison of finite rate model (A) with mass & energy balanced $T_p$ model (B1) for (a) cylinder $(T_p = 655.9K)$ (b) sphere($T_p = 669.9K$).

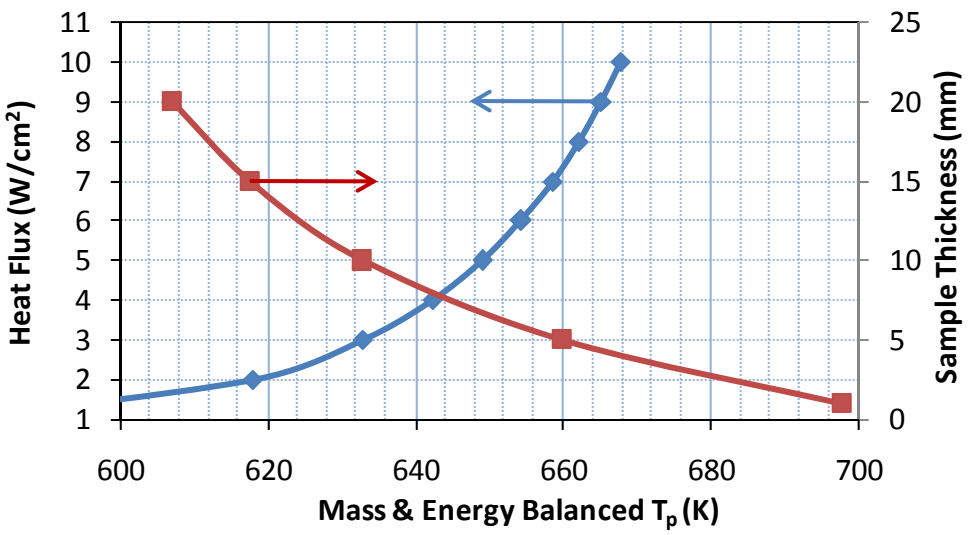


**Figure 4:** Effect of heat flux and sample thickness on energy and mass balanced pyrolysis temperature.

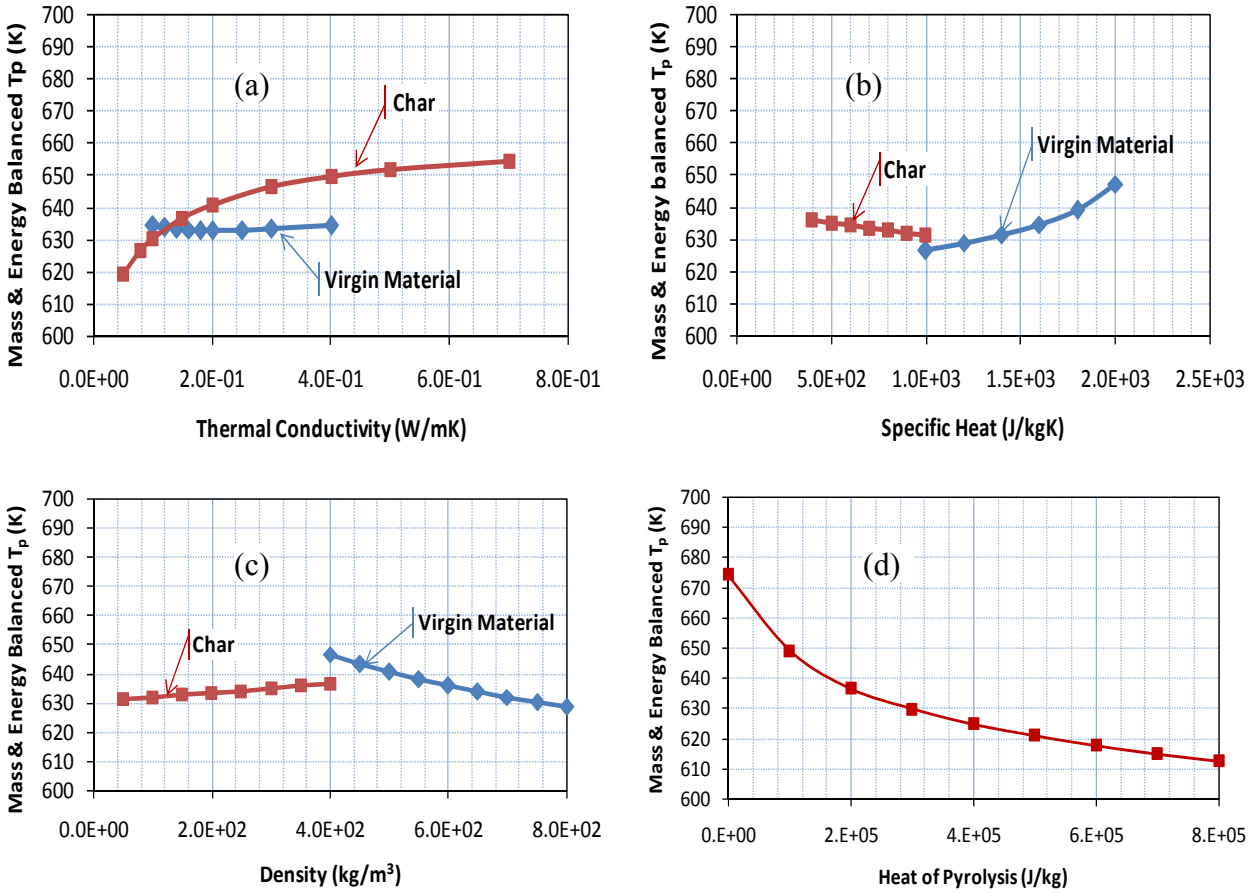


**Figure 5:** Effect of thermal properties of virgin material & char on mass & energy balanced pyrolysis temperature.

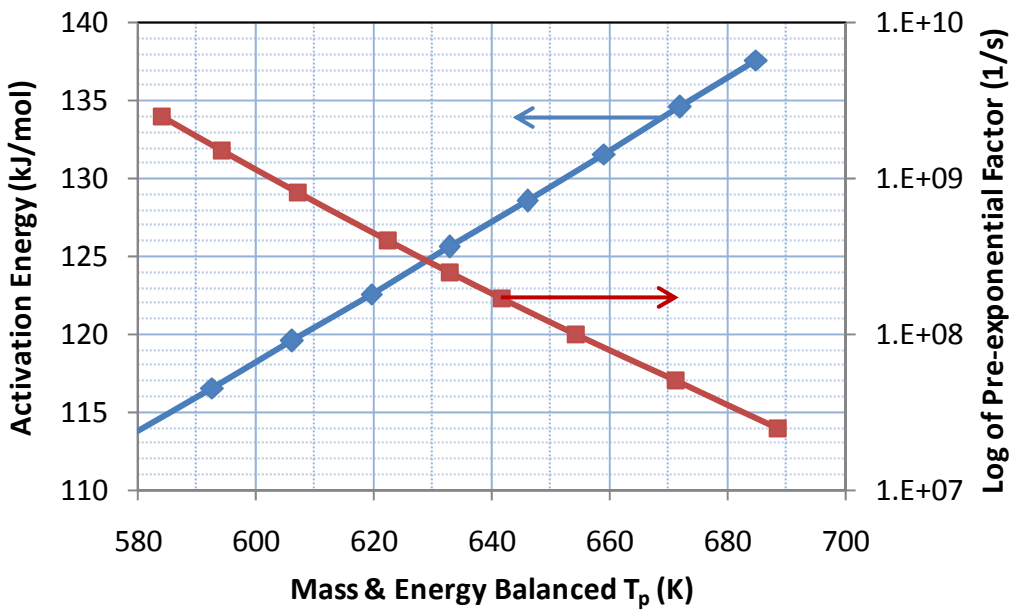


**Figure 6:** Effect of the activation energy & pre-exponential constant on energy and mass balanced $T_p$.

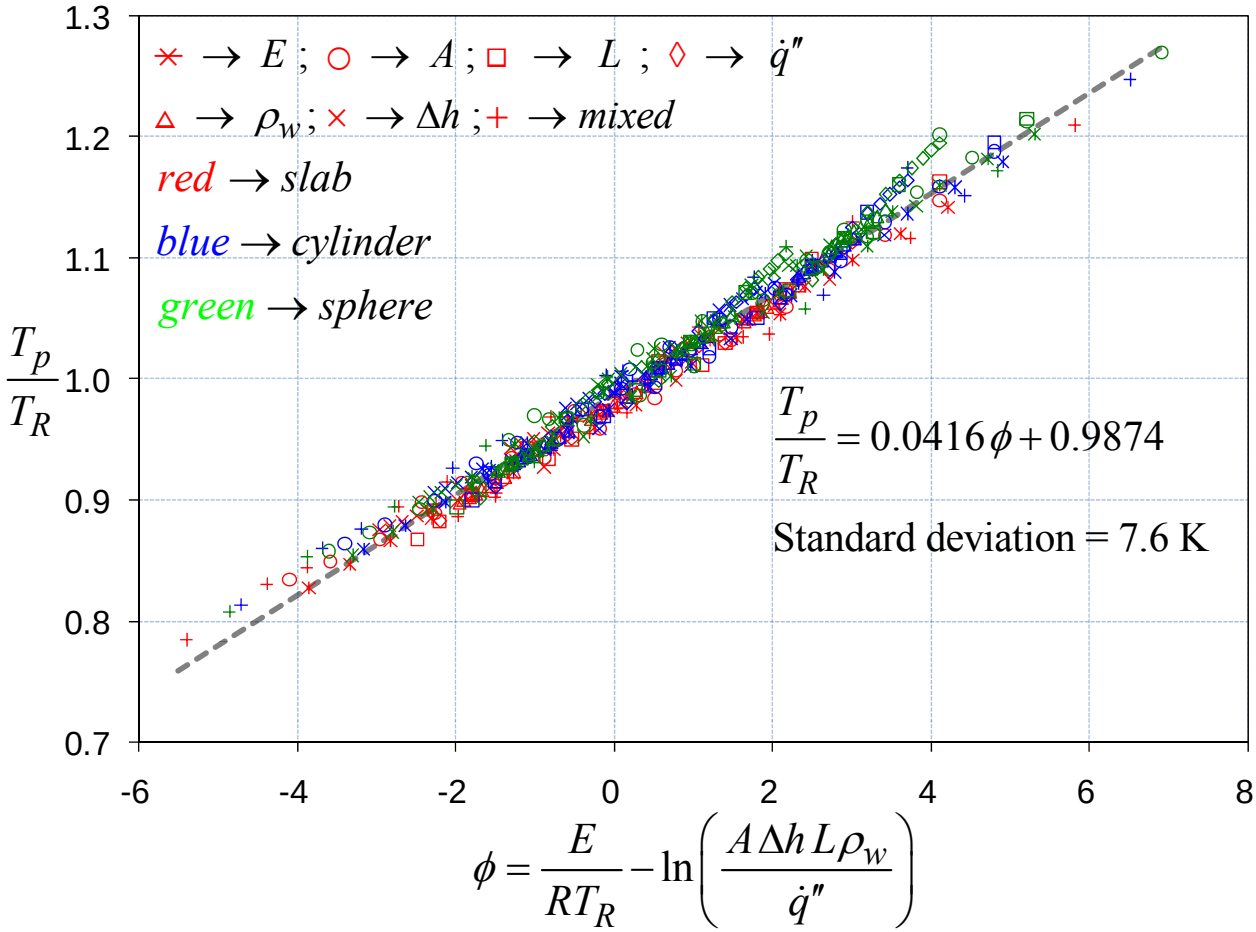


**Figure 7:** Non-dimensional correlation of finite rate and pyrolysis front calculations for a wood slab, cylinder & sphere for estimating the pyrolysis temperature from primary variables namely: Activation energy ($E$); pre-exponential factor ($A$); heat of pyrolysis ($\Delta h$); characteristic thickness ($L$); virgin solid density ($\rho_w$); external heat flux ($\dot{q}''$); and a random mix of these variables. Symbols represent these variables. They were systematically varied over the range available in the literature for wood. The dotted line is the best fit correlation. The correlation is insensitive to the value of the reference temperature ($T_R$) chosen. Here, $T_R$ was varied between $600K$ & $700K$. The standard deviation of the correlation is 7.6K.

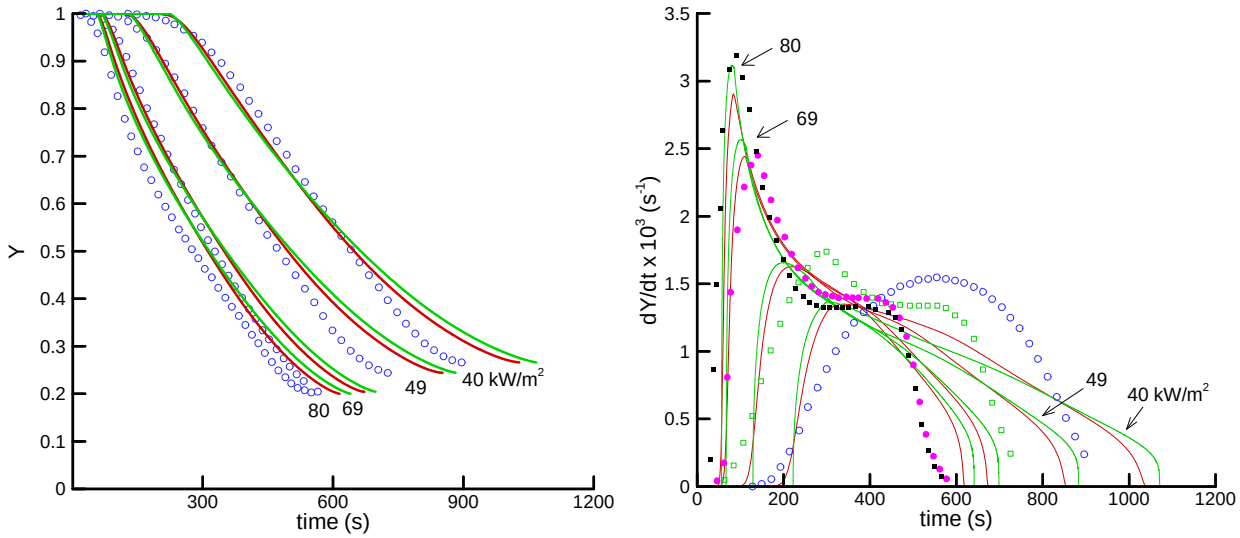


**Figure 8:** Comparison of the models with the experimental measurements of [15]. Symbols – experiments; Red line – finite rate model A; Green line – pyrolysis front model B1. Y → solid mass fraction, dY/dt → solid mass loss rate. Mass & energy balanced $T_p$ for model B1: $\mathbf{642K\ for\ 40\frac{kW}{m^2}; 650K\ for\ 49\frac{kW}{m^2};\ 662K\ for\ 69\frac{kW}{m^2}; 667K\ for\ 80\frac{kW}{m^2}}$.